arXiv:1011.1592v1 [cond-mat.supr-con] 6 Nov 2010

Nanopattern-stimulated superconductor-insulator transition in thin TiN films

T. I. Baturina,[1,2,3] V. M. Vinokur,[3] A. Yu. Mironov,[1] N. M. Chtchelkatchev,[3,4] D. A. Nasimov,[1] and A. V. Latyshev[1,2]

[1] *A. V. Rzhanov Institute of Semiconductor Physics SB RAS, 13 Lavrentjev Avenue, Novosibirsk, 630090 Russia*

[2] *Novosibirsk State University, 2 Pirogova Street, Novosibirsk, 630090 Russia*

[3] *Materials Science Division, Argonne National Laboratory, Argonne, Illinois 60439, USA*

[4] *Institute for High Pressure Physics, Russian Academy of Sciences, Troitsk 142190, Moscow region, Russia*

(Dated: November 9, 2010)

We present the results of the comparative study of the influence of disorder on transport properties in continuous and nanoperforated TiN films. We show that nanopatterning turns a thin TiN film into an array of superconducting weak links and stimulates both, the disorder- and magnetic field-driven superconductor-to-insulator transitions, pushing them to lower degree of disorder. We find that nanopatterning enhances the role of the two-dimensional Coulomb interaction in the system transforming the originally insulating film into a more pronounced insulator. We observe magnetoresistance oscillations reflecting collective behaviour of the multiconnected nanopatterned superconducting film in the wide range of temperatures and uncover the physical mechanism of these oscillations as phase slips in superconducting weak link network.

That a thin film of the same material can be a superconductor but can very well turn an insulator, is one of the most remarkable aspects of disordered superconductors [1–7]. The engine driving the transition between the superconducting and insulating states is disorder the effect of which is two-fold. On the one hand, disorder limits the electron diffusion enhancing thus the Coulomb electron-electron interaction which competes with the Cooper pairing [8, 9]. The latter in an interplay with the disorder-induced inhomogeneities localizes Cooper pairs to form an insulating state, Cooper-pair insulator. A restricted geometry is critical to effects of disorder – for the insulating state to be observed the superconducting material is to be thinned down till its thickness d becomes comparable to or smaller than the superconducting coherence length ξ. One of the major experimental challenges in these studies remains the optimization of material parameters taking it to the closest proximity of the direct superconductor-insulator transition and identifying the systems that exhibit such a transition at available temperatures. In this Letter we meet this challenge via creating a metamaterial with the desirable properties, the multiconnected thin superconducting film. We show that nanopatterning a thin TiN film into a regular sieve-like configuration turns it into an array of weak links and, therefore, stimulates the direct superconductor-to-insulator transition. Depending on the original degree of disorder it either suppresses the critical temperature T_c, or drives the initially superconducting film into an insulating state, or else, transforms the originally insulating film into an even more pronounced insulator.

As a starting material we have chosen a 5 nm thin TiN film which was identical by its parameters to those that experienced the superconductor-insulator transition after soft plasma etching [10–13] and which were fully characterized by the high resolution electron beam, infrared [14], and low-temperature scanning tunnelling spectroscopy [15]. The smooth, continuous, and uniform TiN film was formed on the Si/SiO_2 substrate by atomic layer deposition. The film had the superconducting critical temperature $T_c = 1.03\,\mathrm{K}$, the diffusion constant $D = 0.3\,\mathrm{cm}^2/\mathrm{s}$, and the superconducting coherence length $\xi_d(0) = 9.3\,\mathrm{nm}$. As a first step, the film was patterned into the bridges $50\,\mu\mathrm{m}$ wide and $100\,\mu\mathrm{m}$ long via conventional UV lithography. Then, making use of the electron lithography and the subsequent plasma etching, a square lattice of holes with the diameter $\sim 120\,\mathrm{nm}$ and the period $a = 200\,\mathrm{nm}$ covering the $50 \times 120\,\mu\mathrm{m}^2$ area, was created, see insets in Fig. 1. The voltage probes V1-V2 were designed to fall within the nanopatterned domain of the film, while the probes V3-V4 were placed within its continuous (non-perforated) section to measure thus the resistance of the original continuous film. The perforated section of the film confined between the probes V1-V2 contained $50\,\mu\mathrm{m} \times 100\,\mu\mathrm{m}/(200\,\mathrm{nm})^2 = 125000$ elemental units. To increase the sample sheet resistance, it was sequentially treated by an additional soft plasma etching two times. We will be referring to the untreated sample as to the original one (or as to the state A), discriminating between the non-perforated (i.e. reference) part, rA and the perforated, pA, section of the film. Sequential etching transforms the film into the state B and eventually into the state C, and we will be using the prefixes 'r' and 'p' as in the state A. The room temperature resistances are $3.17\,\mathrm{k}\Omega$ for rA, $3.75\,\mathrm{k}\Omega$ for rB, and $4.76\,\mathrm{k}\Omega$ for rC and $13.87\,\mathrm{k}\Omega$ for pA, $14.45\,\mathrm{k}\Omega$ for pB, and $16.26\,\mathrm{k}\Omega$ for pC. The ratios of the room temperature resistances of the perforated and continuous samples for each respective state is about 3-4, reflecting the approximately 3 times reduction of the effective cross-section of the sample upon perforation. The chosen fabrication procedure allowed studying the evolution of electronic transport properties in a most controllable way avoiding introduction of additional geometric parameters that could vary from sample

to sample. The temperature T- and the magnetic field B-dependences of the resistance were measured using the standard four-probe dc and low frequency ac techniques. The currents were sufficiently small to ensure the linear response regime as was verified by direct measurements of the current-voltage characteristics I-V. The magnetic field was applied perpendicular to the film surface.

We start discussing our results with the zero magnetic field data. Shown in the Fig. 1 are temperature dependences of the resistance per square (to obtain it the measured resistance was divided by two in accordance with the sample aspect ratio) for all three states of the perforated films [panels (a) and (c)] and for the corresponding reference films [panels (b) and (d)]. Both sets demonstrate the superconductor - insulator transitions (SIT). To emphasize on the features of the temperature behaviour of the resistance, we present resistance in both, linear and logarithmic scales, and the temperature in logarithmic sale since it spans over three orders of magnitude. Resistances of all the films grow upon decreasing the temperature from the room temperature down, with all the superconducting samples showing a non-monotonic $R(T)$ behaviour with the pronounced maximum preceding the superconducting transition. So, the maximal resistance of the as-prepared reference superconducting film rA, is $R_{\max} = 5.67\,\mathrm{k\Omega}$. The resistance of the film rB achieves $R_{\max} = 10.3\,\mathrm{k\Omega}$, and for the nanostructured film pA the maximal resistance value becomes $R_{\max} = 39.4\,\mathrm{k\Omega}$ at $T = 1.64\,\mathrm{K}$. On the way down to $T_c = 1.03\,\mathrm{K}$ of the rA film the resistance of the pA sample shows a noticeable decrease to the value of $R = 33.7\,\mathrm{k\Omega}$, which is just about of the resistance per square of the rA film. Upon further cooling the pA sample exhibits the drop in the resistance of about two orders of magnitude. Nevertheless, the pA sample does not transit into a global phase coherent superconducting state, remaining in the resistive state even at lowest temperatures. Deferring the discussion of this feature till after the presentation of the magnetoresistance data, we stress here a striking behaviour of the B-state. While the reference sample rB falls to a superconducting state (although it occurs at $T_c = 0.43\,\mathrm{K}$, which is decreased as compared to that of rA), the nanostructured part pB appears at the insulating state of the SIT. In the state C both, rC and pC are insulating.

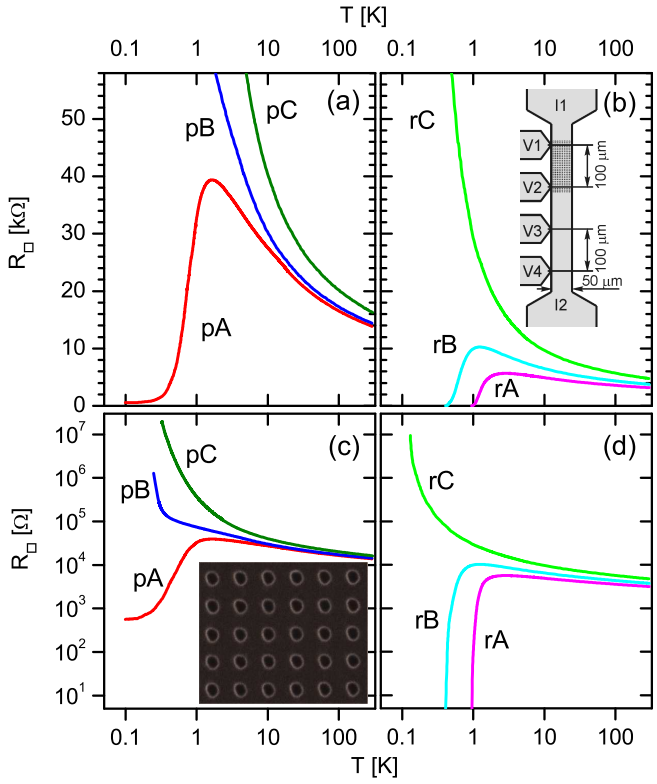

FIG. 1. Resistance per square versus temperature plots displaying superconductor-insulator transitions in the perforated films [panels (a) and (c)] and the corresponding reference films [panels (b) and (d)]. Panels (a) and (b) employ the linear scales of the resistance, whereas in the panels (c) and (d) the logarithmic scales are used. The scales of the resistances are the same pairwise for the (a)-(b) and (c)-(d) panels. The inset to panel (b) sketches the measuring set up (the dimensions shown): I1 and I2 are the current-carrying and the pick up leads, respectively, V1 and V2 leads are attached within the perforated part of the film and V3 and V4 pick up voltage from the original non-perforated section of the film. The inset to panel (c) presents scanning electron microscope (SEM) image of the part of the TiN film patterned with a square array of holes with the diameter $\sim 120\,\mathrm{nm}$ and with the center spacing of 200 nm.

We now turn to details of the electronic transport properties. Upon cooling down to 10 K all samples exhibit logarithmic temperature dependence of the conductance (see Fig. 2a), which is well described by the formula $G(T)/G_{00} = A\ln(k_BT\tau/\hbar)$, where $G(T) = 1/R_\square(T)$ is the conductance, $G_{00} = e^2/(2\pi^2\hbar)$. This behavior is in accord with the theory of quantum corrections for quasi-two-dimensional disordered systems and can be attributed to weak localization and repulsive electron-electron interaction corrections [16]. Similar behaviour was observed before in critically disordered TiN films [15, 17] and in Bi films [3, 18]. Notably, the high-temperature slope is identical for all three samples within each sets (with $A = 2.6 \pm 0.1$ for the reference and $A = 0.85 \pm 0.05$ for perforated films), irrespectively to their low-temperature either superconducting or insulating behaviors. The ratio of the factors A in the reference and perforated parts of the film is close to 3, as expected, due to the geometric reduction of the effective cross sections of the conducting channels in nanopatterned structures as compared to those in the reference films. This evidences that patterning films does not introduce additional microscopic disorder. Thus disorder remains the same in perforated and continuous films for each state, A, B, and C.

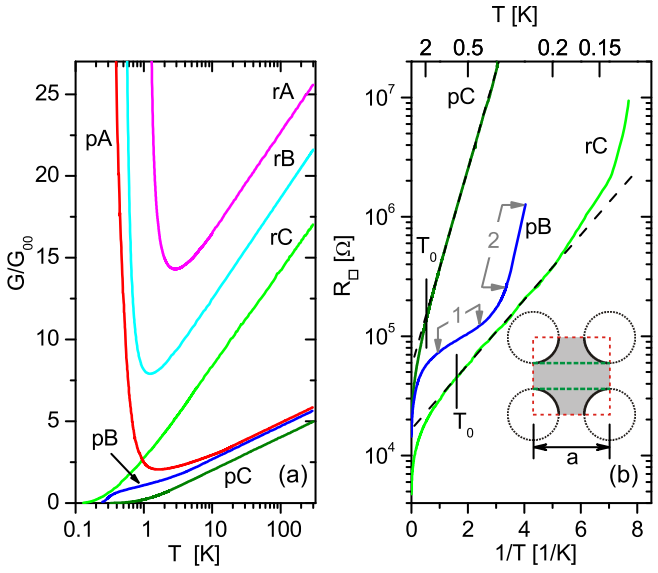

FIG. 2. (a) Conductance $G/G_{00} = 2\pi^2\hbar/(e^2R_\square)$ as function of temperature. Panel (b): $R_\square$ versus $1/T$ dependences for the non-superconducting samples. Both rC and pC show Arrhenius behaviors, the dashed line depicts the fit to Eq. (1) yielding characteristic temperatures $T_0 = 0.63\,\mathrm{K}$ and $1.9\,\mathrm{K}$, and $R_0 = 16.6\,\mathrm{k\Omega}$ and $55.6\,\mathrm{k\Omega}$ for samples rC and pC, respectively. The line bar marks these T_0's emphasizing that T_0's were determined in the domain $T < T_0$ as proper. At lowest temperatures $\log R(T)$ turns upwards departing from the Arrhenius- for *hyperactivated* regime [17]. The behavior of sample pB can not be viewed as the Arrhenius one: Linearisation in the interval 1, going up from $0.4\,\mathrm{K}$ results in $T_0 = 0.35\,\mathrm{K}$, and the Arrhenius law cannot be used for $T > T_0$, while the linearisation in the interval 2 although giving acceptable $T_0 = 2.21\,\mathrm{K}$, results in an unreasonably low $R_0 = 0.15\,\mathrm{k\Omega}$. The inset shows a geometry of an elemental unit of an array, illustrating the reduction of the cross section of the effective conducting channel.

To analyse the behavior of the non-superconducting samples we replot $R(T)$ as function of $1/T$ in Fig. 2b. At low temperatures it is well fitted by the Arrhenius formula for both, the reference and the nanopatterned films in the state C, evidencing that these samples are indeed insulators. The dashed lines correspond to

$$R = R_0 \exp(T_0/T)\,, \qquad (1)$$

with $T_0 = 0.63\,\mathrm{K}$ and $1.9\,\mathrm{K}$ being the characteristic temperatures, and $R_0 = 16.6\,\mathrm{k\Omega}$ and $55.6\,\mathrm{k\Omega}$ for samples rC and pC, respectively. That R_0 of the pC is 3.35 times larger than that of the reference film, paralleled by the ratio of the respective resistances at room temperatures that equals to 3.4, gives more support to observation that patterning does not change the degree of microscopic disorder.

Speaking of the characteristic temperatures, one would have expected that had T_0 been formed over the microscopic scale, it would have remained the same in both reference and perforated films. Instead, one sees a noticeable increase in T_0 in a perforated sample. This suggests that T_0 is built on the macroscopic spatial scales, not less then 200 nm and is influenced by changes in geometric characteristics and the connectivity introduced by patterning. Such a behaviour becomes clear, once one recalls that the characteristic energy of an insulating state of a two-dimensional Josephson junction array (JJA) is $k_\mathrm{B}T_0 = \Delta_\mathrm{c} = E_\mathrm{c}\ln(L/b)$, where E_c is the charging energy of a single superconducting island, L is the smaller quantity out of either the electrostatic screening length of JJA or its linear dimension, and b is the size of the elemental cell of the array [19, 20]. Maintaining that the Cooper-pair-insulating film comprises a self-induced texture of weakly coupled superconducting islands, one would have expected here the same behaviour (the size-dependence of the characteristic energy was observed in the identically prepared TiN films [21] and InO films [22]). Then the upturn in the log $R(T)$ vs. $1/T$ dependence for the rC sample, as well as for the perforated sample pB, occurs at the temperature of the charge Berezinskii-Kosterlitz-Thouless transition (CBKT) $k_\mathrm{B}T_\mathrm{CBKT} \simeq E_\mathrm{c}$; for the rC sample $T_\mathrm{CBKT} \approx 0.14\,\mathrm{K}$. (In artificially manufactured 2D JJA the upturn from the behaviour described by the Eq. (1) due to CBKT was observed in Refs. [23, 24].) This yields $\ln(L/b) = \Delta_\mathrm{c}/E_\mathrm{c} = 4.5$. In Ref. [19] the quantity $b \approx 40\,\mathrm{nm}$ was found for critically disordered TiN films in the vicinity of the SIT, corresponding to $b \approx 4\xi$. We, thus, obtain $L \approx 3.4\,\mu\mathrm{m}$, and, since this value is apparently less then the size of the sample of $50\,\mu\mathrm{m}$ (but at the same time well exceeds 200 nm), L represents the electrostatic screening length. To crudely estimate the effect of perforation we assume the originally square Josephson network with the lattice constant $\approx 40\,\mathrm{nm}$ and notice that perforation transforms this network into the new one with the 'bond' length equal to 200 nm, each bond comprising a series of five junctions. This straightforwardly gives an estimate for new characteristic energy $\tilde{\Delta}_\mathrm{c} = 5\Delta_\mathrm{c} - 5E_\mathrm{c}\ln 5 = 2\,\mathrm{K}$, which nicely agrees with the experimental finding of $1.9\,\mathrm{K}$ for the characteristic energy for the sample pC. The increase in the characteristic energy upon removing the fraction of the junctions of the 2D JJA was found in [24].

Applying magnetic field to nanopatterned films brings in competing energy- and spatial scales and thus commensurability effects which manifest themselves through the oscillations in thermodynamics and transport properties. Shown in Fig. 3 are the magnetoresistance data for the pA sample at relatively weak magnetic field, over the range $\pm 0.5\,\mathrm{T}$, which is much less than the upper critical field of the reference film (the reference film is close by its parameters to the low resistive sample of Ref. [10]) $B_{c2} = 2.8\,\mathrm{T}$. There are eight pronounced magnetoresistance (MR) oscillations at low temperatures (for each polarity of the field). The main period is $B_0 = \Phi_0/a^2$, where $\Phi_0 = \pi\hbar/e$ is the superconduct-

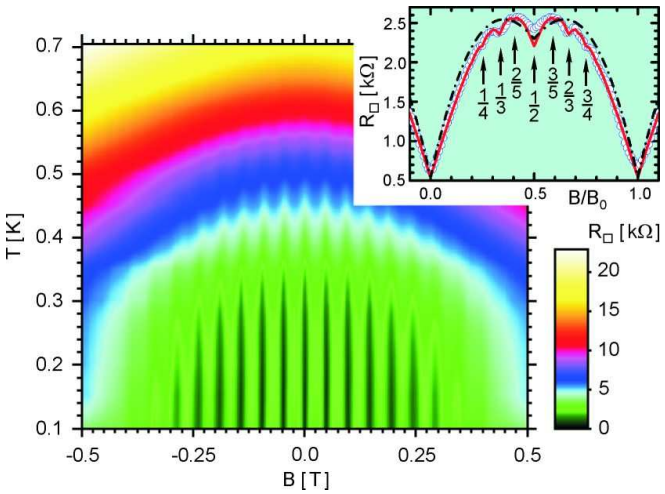

FIG. 3. The two-dimensional colour map of the resistance in the temperature - magnetic field plane for the perforated sample pA. The colour scale quantifying magnitudes of the resistance is given at the lower right corner. The inset shows the experimental data of the magnetoresistance (open circles) vs. reduced magnetic field B/B_0, where $B_0 = \Phi_0/a^2$, at temperature 0.11 K. In addition to the fundamental dips at $B_n = B_0$, where n is an integer, the secondary dips at $B/B_0 = 1/4$, $1/3$, $2/5$, $1/2$, $3/5$, $2/3$, and $3/4$ are observed. Dash-dotted line corresponds to the periodic dependence of the fractional reduction in average Josephson coupling energy on the magnetic flux per unit cell derived in the nearest-neighbour contour approximation of Ref. [29]. The solid line passes through the theoretical values calculated for rational $B/B_0 = p/q$, with $q \leq 256$, on the superconducting network Eq. (2) accounting for multi-contour phase synchronization and thus exhibiting higher order commensurability effects.

ing flux quantum, corresponding one flux quantum per unit cell. Magnification of the resistive curve (see inset in Fig. 3) reveals a fine structure reflecting collective behaviour of the multiconnected superconducting film differing it from the behavior of a single superconducting loop. One distinguishes additional well-defined dips at $B/B_0 = 1/4$, $1/3$, $2/5$, $1/2$, $3/5$, $2/3$, and $3/4$. The previous observations reported the $B/B_0 = 1/2$ feature in square Josephson junction arrays [25–28], proximity-effect junction arrays [29–32], perforated films and superconducting wire networks [33–36]. The "full" set of dips was observed in the MR of square JJA [27, 28] and in proximity-effect junction arrays [32] and in the critical temperature variation in square superconducting wire network [33].

A description of the observed modulated MR is based on the solution of the Ginzburg-Landau equation on the superconducting network in the presence of the magnetic field [33]. The wave function ψ for the square superconducting network follows the so-called Harper equation [37]:

$$\psi_{n+1} + \psi_{n-1} + 2\cos(2\pi\Phi n + \alpha)\psi_n = \epsilon\psi_n\,. \qquad (2)$$

Here magnetic field B appears through the flux per plaquette $Ba^2/\Phi_0 \equiv \Phi/\Phi_0 = p/q$, where p and q are relative prime numbers. The matrix, corresponding to this equation has $q \times q$ dimensions. The fields at which resistivity exhibits the dips are defined by the boundaries of the energy spectrum as function of the magnetic field, i.e. one has to find $E(\Phi) = \max_\alpha[\epsilon(\Phi, \alpha)]$. To this end we decompose the matrix discriminant into the polinomial of ε independent on α and the offset function independent on ε [38]. The change in the magnetoresistance is calculated as $\Delta R(B) = A \arccos^2[E(\Phi)/4]$, where A is a numerical coefficient, which does not depend on the magnetic field. The resulting $\Delta R(B)$ behaviour is shown by the solid line in the Fig. 3 and demonstrates an excellent agreement with the data at low temperatures. The half-flux dip results mainly from the contribution from the currents in the adjacent loops as it was shown in Ref. [29]. As temperature increases the fine structure is smeared out, while the oscillations with the main period B_0 persist till $T \simeq 0.7$ K, where they are easily resolved by taking dR/dB.

The most intriguing aspect of the observed MR oscillations is an extremely wide temperature region of their presence. The MR oscillations in the perforated films and/or superconducting wire networks (SWN), were usually found, if measured in the linear response regime, in the close proximity to T_c in the region $\Delta T \lesssim 0.02T_c$ [33, 34, 39–43]. More extended temperature regions of the MR oscillations were reported in Refs. [35, 36, 44–48]. Juxtaposing the data obtained for various systems and inspecting the systems' geometric characteristics we observe that as a rule the low-temperature boundary for the MR oscillations to appear corresponds to the temperature at which the ratio $w/\xi_{\rm d}(T) \lesssim 5$, where w is the width of the superconducting constriction and $\xi_{\rm d}(T) = \xi_{\rm d}(0)/\sqrt{1 - T/T_{\rm c}}$. This brings to the mind the Likharev's result [49] that the weak link cannot accommodate an Abrikosov vortex if $w < w_{\rm c}$ and transforms into a Josephson junction, where the critical width $w_{\rm c}(L)$ was evaluated as being equal to $4.41\xi(T)$ for the long, $L \gg w$, link (L is the link length) near $T_{\rm c}$. For the square link, $L = w$, $w_{\rm c} \approx 5\xi$ and can become well larger for the short weak links. In order to gain the insight into the meaning of the boundary separating the dissipative behaviour governed by the vortex motion from the resistive state due to phase slips, let us employ the approach used in [50] to evaluate the condition of clustering of vortex cores. Namely, note that either in the presence of the magnetic field or upon passing the current, superconductivity near the edges of the constriction is suppressed and the Andreev states separated by minigaps $\simeq \Delta/(k_{\rm F}\xi)$ should form. Due to overlap of the wave functions localized at the opposite edges these states broaden as $\Delta \exp(-w/\xi)$. At the width $w_0 \simeq \xi \ln(k_{\rm F}\xi)$, where the quasiparticle levels broadening becomes of the order of the level separation, the constriction turns metal-

lic and start to behave as a proximity effect generated Josephson junction. The estimate for w_0 (at the plausible values of k_F and ξ) is in a reasonable agreement with the all available experimental data and gives the ratio $w_0/\xi(T) \simeq 4 \div 8$. Note that the above qualitative consideration does not use closeness to T_c and implies that the concept of the critical size of the superconducting weak link below which it turns into a Josephson junction can be extended to low temperatures.

The next observation is that in order to exhibit oscillations in the magntoresistance, the SWN should be in a resistive state. Thus the second condition determining the 'range of observability' of the oscillations is that the temperature should be higher than the temperature of the vortex BKT transition in the SWN, T_{VBKT}. Using the magnitude of the critical current observed in our experiment at $T = 0.1\,K$ evaluated from the position of the maximum of the dV/dI vs. I curve [32], $I_c = 0.17\,\mu A$, giving $I_{c(i)} = 0.68\,nA$ per one constriction, one obtains the Josephson coupling energy as $E_J/k_B = 0.016\,K$. Therefore, indeed, even the lowest temperature of our experiment (0.1 K), where the MR oscillations are clearly detectable, lie in the interval $T > T_{VBKT} = \pi E_J/(2k_B)$ [51]. For this reason the $R_\square(T)$ dependence for the pA sample remains finite at all the experimental temperatures.

Finally, we briefly discuss the MR at large fields beyond the range of oscillations for the pA sample. At fields slightly larger than the critical field $B_{c2} = 2.8\,T$ of the reference film [10], we observe a huge peak of the MR at some $B = B_{max}$, followed by the appreciable negative MR, as shown at the right inset in Fig. 4. The value of B_{max} shifts towards larger fields upon increase in T. The similar shifts of the maxima and the subsequent negative MR are observed in the reference film (see Fig. 1c of Ref. [10]) and are well described by the quantum corrections to the conductivity due to superconducting fluctuations [52]. The main panel of Fig. 4 shows the evolution of the $R_\square(T)$ dependences at different magnetic fields. At zero field there is a high temperature, $T = 1.64\,K$, maximum (Fig. 1). At higher fields, but not too far beyond $B \approx 2\,T$, a second, low temperature maximum appears. At yet higher fields, as B approaches and further exceeds B_{c2} of the reference film, the $R_\square(T)$-dependences become monotonically decreasing with the temperature increase. Notably, in spite of the fact that the MR exhibits huge peak, up to $200\,k\Omega$ per square at 0.1 K, it can be hardly viewed as the manifestation of the magnetic-field-induced superconductor-insulator transition. Indeed, the conductance $G(T) = 1/R_\square(T)$ at fields around and above the peak, fits perfectly to the logarithmic temperature dependence $G(T)/G_{00} = A\ln(k_B T\tau/\hbar)$, see left inset in Fig. 4, with A monotonically decreasing with the growth of the magnetic field, $A = 0.49$, 0.45, and 0.38 at fields 2.5, 3.0, and 11.0 T, respectively. This decrease is likely to reflect the suppression of the contribution from the superconducting fluctuations to conductivity. Moreover, we observe that the value of $A = 0.38$, being multiplied by the geometry factor of 3, becomes equal to 1.14, which is pretty close $A = 1$ expected for the contribution to the conductivity of disordered metals due to the repulsive electron-electron interaction [16]. We conclude that although this sample does not exactly exhibits the magnetic field driven SIT, it still demonstrates the significant amplification of the resistivity growth with the decreasing temperature (the resistance increases by almost the factor of 3.5 in the interval from 1 to 0.1 K at $B = 3\,T$, while in the reference film the corresponding factor is about 1.4), and thus can be considered as being put at the threshold of the transition from the weak to strong localization by nanopatterning.

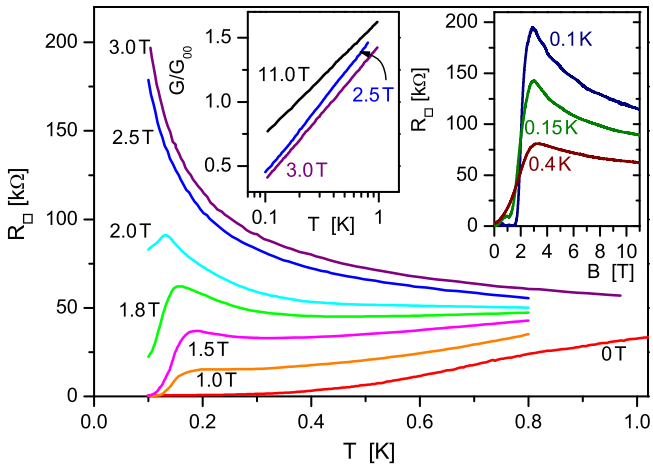

FIG. 4. The resistance per square versus temperature plots in the magnetic fields $B = 0$, 1.0, 1.5, 1.8, 2.0, 2.5, 3.0 T for the perforated sample pA. Left inset: The conductance $G/G_{00} = 2\pi^2\hbar/(e^2 R_\square)$ as a function of the temperature in a logarithmic scale in the magnetic fields $B = 2.5$, 3.0, and 11.0 T. Right inset: Magnetoresistance isotherms at temperatures $T = 0.1$, 0.15, and 0.4 K. The positions of maxima are $B_{max} = 2.9$, 3.0, and 3.3 T, correspondingly.

We are delighted to thank Boris Shapiro (Bar-Ilan University) and Alexander Mel'nikov for useful discussions. This research is supported by the Program "Quantum Physics of Condensed Matter" of the Russian Academy of Sciences, by the Russian Foundation for Basic Research (Grant No. 09-02-01205), and by the U.S. Department of Energy Office of Science under the Contract No. DE-AC02-06CH11357.

[1] M. Strongin, R. S. Thompson, O. F. Kammerer, and J. E. Crow, Phys. Rev. B **1**, 1078 (1970).

[2] D. B. Haviland, Y. Liu, and A. M. Goldman, Phys. Rev. Lett. **62**, 2180 (1989).

[3] Y. Liu, D. B. Haviland, B. Nease, and A. M. Goldman, Phys. Rev. B **47**, 5931 (1993).

[4] A. M. Goldman and N. Marković, Phys. Today **51**(11), 39 (1998).

[5] E. Bielejec, J. Ruan, and W. Wu, Phys. Rev. Lett. **87**, 036801 (2001).

[6] N. Hadacek, M. Sanquer, and J.-C. Villégier, Phys. Rev. B **69**, 024505 (2004).

[7] Y. Qin, C. L. Vicente, and J. Yoon, Phys. Rev. B **73**, 100505(R) (2006).

[8] S. Maekawa and H. Fukuyama, J. Phys. Soc. Jpn. **51**, 1380 (1982).

[9] A. M. Finkel'stein, Sov. Phys. JETP Lett. **45**, 37 (1987); Physica B **197**, 636 (1994).

[10] T. I. Baturina, J. Bentner, C. Strunk, M. R. Baklanov, A. Satta, Physica B **359**, 500 (2005).

[11] T. I. Baturina, C. Strunk, M. R. Baklanov, and A. Satta, Phys. Rev. Lett. **98**, 127003 (2007).

[12] T. I. Baturina, A. Yu. Mironov, V. M. Vinokur, M. R. Baklanov, and C. Strunk, Phys. Rev. Lett. **99**, 257003 (2007).

[13] T. I. Baturina, A. Bilušić, A. Yu. Mironov, V. M. Vinokur, M. R. Baklanov, and C. Strunk, Physica C **468**, 316 (2008).

[14] F. Pfuner, L. Degiorgi, T. I. Baturina, V. M. Vinokur, and M. R. Baklanov, New Journal of Physics **11**, 113017 (2009).

[15] B. Sacépé, C. Chapelier, T. I. Baturina, V. M. Vinokur, M. R. Baklanov, and M. Sanquer, Phys. Rev. Lett. **101**, 157006 (2008); preprint arXiv:0906.1193.

[16] B. L. Altshuler and A. G. Aronov, in: *Electron-Electron Interactions in Disordered Systems*, ed. by A. L. Efros and M. Pollak (North-Holland, Amsterdam, 1985).

[17] T. I. Baturina, A. Yu. Mironov, V. M. Vinokur, M. R. Baklanov, and C. Strunk, JETP Lett. **88**, 752 (2008).

[18] J. A. Chervenak and J. M. Valles, Jr., Phys. Rev. B **59**, 11209 (1999).

[19] M. V. Fistul, V. M. Vinokur, and T. I. Baturina, Phys. Rev. Lett. **100**, 086805 (2008).

[20] V. M. Vinokur, T. I. Baturina, M. V. Fistul, A. Yu. Mironov, M. R. Baklanov, and C. Strunk, Nature **452**, 613 (2008).

[21] D. Kalok, A. Bilušić, T. I. Baturina, V. M. Vinokur, and C. Strunk, to be published.

[22] D. Kowal and Z. Ovadyahu, Physica C **468**, 322 (2008).

[23] A. Kanda and S. Kobayashi, J. Phys. Soc. Jpn. **64**, 19 (1995).

[24] T. Yamaguchi, R. Yagi, S. Kobayashi, and Y. Ootuka, J. Phys. Soc. Jpn. **67**, 729 (1998).

[25] R. A. Webb, R. F. Voss, G. Grinstein, and P. M. Horn, Phys. Rev. Lett. **51**, 690 (1983).

[26] B. J. van Wees, H. S. J. van der Zant, and J. E. Mooij, Phys. Rev. B **35**, 7291 (1987).

[27] H. S. J. van der Zant, F. C. Fritschy, W. J. Elion, L. J. Geerligs, and J. E. Mooij, Phys. Rev. Lett. **69**, 2971 (1992).

[28] H. S. J. van der Zant, W. J. Elion, L. J. Geerligs, and J. E. Mooij, Phys. Rev. B **54**, 10081 (1996).

[29] M. Tinkham, D. W. Abraham, and C. J. Lobb, Phys. Rev. B **28**, 6578 1983.

[30] D. Kimhi, F. Leyvras, and D. Ariosa, Phys. Rev. B **29**, 1487 (1984).

[31] M. G. Forrester, Hu Jong Lee, M. Tinkham, and C. J. Lobb, Phys. Rev. B **37**, 5966 (1988).

[32] S. P. Benz, M. S. Rzchowski, M. Tinkham, and C. J. Lobb, Phys. Rev. B **42**, 6165 (1990).

[33] B. Pannetier, J. Chaussy, R. Rammal, and J. C. Villegier, Phys. Rev. Lett. **53**, 1845 (1984).

[34] L. Van Look, B. Y. Zhu, R. Jonckheere, B. R. Zhao, Z. X. Zhao, and V. V. Moshchalkov, Phys. Rev. B **66**, 214511 (2002).

[35] T. I. Baturina, D. W. Horsell, D. R. Islamov, I. V. Drebushchak, Yu. A. Tsaplin, A. A. Babenko, Z. D. Kvon, A. K. Savchenko, A. E. Plotnikov, Physica B **329**, 1496 (2003).

[36] T. I. Baturina, Yu. A. Tsaplin, A. E. Plotnikov, M. R. Baklanov, Physica B **378**, 1058 (2006).

[37] P. G. Harper, Proc. Phys. Soc. London A **68**, 874 (1955).

[38] C. Kreft, TU-Berlin, SFB 288, Preprint No. 89 (1993).

[39] A. T. Fiory, A. F. Hebard, and S. Somekh, Appl. Phys. Lett. **32**, 73 (1978).

[40] A. Hoffmann, P. Prieto, and I. K. Schuller, Phys. Rev. B **61**, 6958(R) (2000).

[41] U. Patel, Z. L. Xiao, J. Hua, T. Xu, D. Rosenmann, V. Novosad, J. Pearson, U. Welp, W. K. Kwok, and G. W. Crabtree, Phys. Rev. B **76**, 020508(R) (2007).

[42] S. Avci, Z. L. Xiao, J. Hua, A. Imre, R. Divan, J. Pearson, U. Welp, W. K. Kwok, and G. W. Crabtree, Appl. Phys. Lett. **97**, 042511 (2010).

[43] Ajay D. Thakur, Shuuichi Ooi, Subbaiah P. Chockalingam, John Jesudasan, Pratap Raychaudhuri, and Kazuto Hirata, Appl. Phys. Lett. **94**, 262501 (2009).

[44] H. Q. Nguyen, S. M. Hollen, M. D. Stewart, Jr., J. Shainline, Aijun Yin, J. M. Xu, and J. M. Valles, Jr., Phys. Rev. Lett. **103**, 157001 (2009).

[45] S. Ooi, T. Mochiku, S. Yu, E. S. Sadki, K. Hirata, Physica C **426**, 113 (2005).

[46] A. Yu. Mironov, T. I. Baturina, V. M. Vinokur, S. V. Postolova, P. N. Kropotin, M. R. Baklanov, D. A. Nasimov, A. V. Latyshev, Physica C (2010), doi:10.1016/j.physc.2009.12.057.

[47] I. Sochnikov, A. Shaulov, Y. Yeshurun, G. Logvenov, and I. Božović, Nature Nanotechnology **5**, 516 (2010).

[48] I. Sochnikov, A. Shaulov, Y. Yeshurun, G. Logvenov, and I. Božović, Phys. Rev. B **82**, 094513 (2010).

[49] K. K. Likharev, Rev. Mod. Phys. **51**, 101 (1979).

[50] A. S. Mel'nikov and M. A. Silaev, JETP Lett. **83**, 578 (2006).

[51] C. J. Lobb, D. W. Abraham, and M. Tinkham, Phys. Rev. B **27**, 150 (1983).

[52] V. M. Galitski and A. I. Larkin, Phys. Rev. B **63**, 174506 (2001).